Enhanced Adaptive Downlink Transmission in MIMO-OFDM Systems by Hardware-Based Calibration

Markus Stefer*, Mark Petermann†, Martin Schneider*, Dirk Wübben†, Karl-Dirk Kammeyer†

*RF & Microwave Engineering Laboratory
Email:{markus.stefer, martin.schneider}@hf.uni-bremen.de
†Department of Communications Engineering
Email:{petermann, wuebben, kammeyer}@ant.uni-bremen.de
University of Bremen, 28359 Bremen, Germany

Abstract— In this paper, a hardware-based calibration scheme at the base station is used to mitigate the impact of the non-reciprocal transceivers in a time division duplex (TDD) multiple-input-multiple-output orthogonal-frequency-division-multiplexing (MIMO-OFDM) system. The calibration setup consists of two single-pole-double-throw (SPDT) switches to bypass the calibration and the data signals. Additionally, an attenuator is needed to avoid overdriving the receive chain of the transceivers. Simulation results show that this calibration scheme results in lower bit error rate (BER) values of the communication system. These results are underlined by measurement results exploiting the low-cost and simple-technology calibration solution.

I. INTRODUCTION

To be able to serve the demand for increasing data rates adaptive communication systems are of great interest. The state of the art transmission strategy is the orthogonal frequency division multiplexing (OFDM) technique due to its ability of adapting to frequency-selective channels [1]. The reciprocity of the physical radio frequency channel suggests to exploit the uplink (UL) channel state information (CSI) for adaptive transmission strategies in the downlink (DL) for a time division duplex (TDD) based system [2]. Conversely, the reciprocity theorem does not hold for the corresponding baseband to baseband communication because of the non-reciprocal transceivers at the base station (BS) and the mobile subscribers (MS). The transceivers have to be considered as non-reciprocal because different components are used for assembling the receive and transmit chains including the digital-to-analog converter (DAC) and analog-to-digital converter (ADC) [3]. However, the effect of non-reciprocal transceivers

can be reduced by exploiting calibration schemes leading to an improved performance in terms of the BER. In [4], a low-cost calibration setup was sketched and the relative calibration procedure was explained and compared with an earlier proposed setup [3] in terms of cost effectiveness. The latter setup has been proven to work by comparing the resulting QAM constellation diagrams before and after applying the calibration. In [5], an experimental investigation of a TDD system based on Zero-Forcing pre-equalization is executed. The author also uses a calibration procedure which relies on a calibration setup similar to that described in [4]. Our contribution is the manufacture of a calibration setup based on this low-cost calibration solution [4] and its evaluation with the help of our data transmission link. This link consists of a multiple antenna demonstrator [6] and a software framework exploited in [7] to demonstrate the influence of non-reciprocal transceivers on the BER. Using our manufactured calibration setup and an appropriate calibration procedure, it is possible to achieve a mitigation of the multi-user interference, which will be explained in the remainder of the paper.

The paper is structured as follows. The system model including the linear pre-equalization techniques and the calibration procedure as well as the modeling of the non-reciprocal transceivers is explained in Section II. Subsequently, simulation results are presented and discussed in Section III. The measurement setup including the calibration and measurement results are described in Section IV followed by concluding remarks in Section V.

Throughout this paper, $(\bullet)^T$ denotes the transpose, $(\bullet)^H$ the conjugate transpose, $(\bullet)^*$ the complex conjugate, tr $\{\bullet\}$ the trace of a matrix, $(\bullet)^{-1}$ the inverse and the Moore-Penrose pseudoinverse is denoted by $(\bullet)^\dagger$. The notation $|\bullet|^2$ translates into taking the squared magnitude of every single matrix entry

separately. Boldface capital letters denote matrices, boldface lower-case letters denote vectors and lower-case letters denote scalars.

II. SYSTEM MODEL AND CALIBRATION PROCEDURE

First, the system model for the multiuser-multiple-input-single-output-OFDM (MU-MISO-OFDM) system based on pre-equalization will be introduced. With respect to the pre-equalization schemes taken from [8], this is identical to a MIMO-OFDM system. The main difference though are the non-cooperative users. The proposed model [9], [10] accounts for the front-end effects and also includes calibration matrices to compensate for the non-reciprocal transceivers at the base station. The calibration procedure [4] is explained in subsection II-B which provides the parameters needed to set up the calibration matrices.

A. System Model

In [9], scattering parameters are used to model the front-end devices and multiple antennas in a mobile communication system. This model is able to include all effects that might be present in a mobile communication system such as imperfect matching of the receive and transmit chains of the transceivers and the mutual coupling of multiple antennas, e.g., at the base station. Assuming well-matched transceivers, the downlink and the uplink channel matrix $\mathbf{H}_{\mathrm{DL},k}$ and $\mathbf{H}_{\mathrm{UL},k}$ including the transmit and receive chains at the BS and the MS are given by [9]

$$\mathbf{H}_{\mathrm{DL},k} = \mathbf{G}_{\mathcal{M}\,\mathrm{R},k} \cdot \mathbf{H}_k \cdot \mathbf{G}_{\mathcal{B}\,\mathrm{T},k} \qquad (1)$$

$$\mathbf{H}_{\mathrm{UL},k} = \mathbf{G}_{\mathcal{B}\,\mathrm{R},k} \cdot \mathbf{H}_k^T \cdot \mathbf{G}_{\mathcal{M}\,\mathrm{T},k} \qquad (2)$$

where k denotes the subcarrier index. In (1) and (2), $\mathbf{H}$ denotes the physical MIMO DL channel and the transmit and receive chains are assembled in the diagonal matrices $\mathbf{G}_{\{\mathcal{BM}\}\,\mathrm{T},k}$ and $\mathbf{G}_{\{\mathcal{BM}\}\,\mathrm{R},k}$, respectively. With the aforementioned description of the uplink and downlink channel matrices, the following equation can be set up to describe the investigated adaptive multiuser-MISO-OFDM system with N_{sc} subcarriers which exploits pre-equalization with filter matrix $\mathbf{F}_{\{\mathrm{ZF},\mathrm{WF}\},k}$ [8]

$$\hat{\mathbf{d}}_k = \mathbf{H}_{\mathrm{DL},k} \cdot \mathbf{F}_{\{\mathrm{ZF},\mathrm{WF}\},k} \cdot \mathbf{d}_k + \beta_{\{\mathrm{ZF},\mathrm{WF}\},k}^{-1} \cdot \mathbf{n}_k , \qquad (3)$$

with $\mathbf{F}_{\{\mathrm{ZF},\mathrm{WF}\},k} = \mathbf{C}_k \cdot \mathbf{F}_{\mathrm{pre},\{\mathrm{ZF},\mathrm{WF}\},k}$. Here, $\mathbf{C}_k$ denotes the calibration matrix, which includes the results of the relative calibration procedure, and the actual pre-equalization filter is denoted by $\mathbf{F}_{\mathrm{pre},\{\mathrm{ZF},\mathrm{WF}\},k}$. The power scaling factor $\beta_{\{\mathrm{ZF},\mathrm{WF}\},k}$

in (3) accounts for a constrained transmit power $P_{\mathrm{T},k}$. For the sake of a simplified notation, the subcarrier index k will be dropped for the remainder of this subsection. The pre-equalization filter regarding Zero-Forcing exploiting the uplink matrix is represented by [8]

$$\mathbf{F}_{\mathrm{pre},\mathrm{ZF}} = \left(\mathbf{H}_{\mathrm{UL}}^T\right)^{\dagger}$$
$$= \mathbf{G}_{\mathcal{B}\,\mathrm{R}}^* \mathbf{H}^H \left[\mathbf{H}\,|\mathbf{G}_{\mathcal{B}\,\mathrm{R}}|^2\,\mathbf{H}^H\right]^{-1} \cdot \mathbf{G}_{\mathcal{M}\,\mathrm{T}}^{-1} \quad (4)$$

and the Wiener pre-equalization filter [8] is given by (5) on top of the next page. The power scaling factor is obtained by

$$\beta_{\{\mathrm{ZF},\mathrm{WF}\}} = \sqrt{P_{\mathrm{T}}/\mathrm{tr}\left\{\mathbf{F}_{\{\mathrm{ZF},\mathrm{WF}\}}^H \cdot \mathbf{F}_{\{\mathrm{ZF},\mathrm{WF}\}}\right\}}. \quad (6)$$

B. Calibration Procedure

Due to non-reciprocal transceivers, the product $\mathbf{G}_{\mathcal{B}\,\mathrm{T},k}\,\mathbf{G}_{\mathcal{B}\,\mathrm{R},k}^{-1}$ inhibits the intended pre-equalization, which yields a remaining multiuser interference. This can also be extracted from (7) and (8), which are obtained by rearranging the product $\mathbf{V}_{\{\mathrm{ZF},\mathrm{WF}\},k} = \mathbf{H}_{\mathrm{DL},k}\,\mathbf{C}_k\,\mathbf{F}_{\mathrm{pre},\{\mathrm{ZF},\mathrm{WF}\},k}$ (see next page, subcarrier index is also dropped). The two equations assemble the pre-equalization filter matrix, the calibration matrix and the downlink channel matrix to deduce a calibration specification. The latter is accomplished by designing the diagonal matrix $\mathbf{C}_k$ with entries $c_{1k}, \ldots, c_{nk}$ such that

$$\mathbf{G}_{\mathcal{B}\,\mathrm{T},k} \cdot \mathbf{C}_k \cdot \mathbf{G}_{\mathcal{B}\,\mathrm{R},k}^{-1} = \zeta_k \cdot \mathbf{I} \qquad (9)$$

holds, and the c_{ik} with $i = 1, \ldots, n$ are therefore given by

$$c_{ik} = \zeta_k \cdot \frac{g_{\mathcal{B}\,\mathrm{R},ik}}{g_{\mathcal{B}\,\mathrm{T},ik}}. \qquad (10)$$

Here, transceiver 1 of the BS acts as the reference, which specifies ζ_k to be equal to $\zeta_k = g_{\mathcal{B}\,\mathrm{T},1k}/g_{\mathcal{B}\,\mathrm{R},1k}$. Since (7) and (8) are valid for one subcarrier k, N_{sc} calibration matrices have to be established. The specific calibration parameters are obtained by executing the calibration procedure depicted in Fig. 1, where a known OFDM symbol is transmitted from transmitter 1 (Tx 1) to receiver 2 (Rx 2) via the calibration setup to gather the transfer function $\mathbf{t}_{21}$. Secondly, a known OFDM symbol is transmitted from transmitter 2 (Tx 2) to receiver 1 (Rx 1) via the calibration setup to determine the transfer function $\mathbf{t}_{12}$. Finally, the fraction $\mathbf{t}_{12}/\mathbf{t}_{21}$ provides the calibration parameters $\mathbf{c_2}$ of the N_{sc} subcarriers. Here, it has to be pointed out that the application of this calibration scheme presumes an

$$\mathbf{F}_{\text{pre,WF}} = \mathbf{G}_{\mathcal{B}\text{R}}^* \, \mathbf{H}^H \left[\mathbf{H} \, |\mathbf{G}_{\mathcal{B}\text{R}}|^2 \, \mathbf{H}^H + \frac{\sigma_n^2}{P_\text{T}} \left(|\mathbf{G}_{\mathcal{M}\text{T}}|^2 \right)^{-1} \right]^{-1} \mathbf{G}_{\mathcal{M}\text{T}}^{-1} \tag{5}$$

$$\mathbf{V}_{\text{ZF}} = \mathbf{G}_{\mathcal{M}\text{R}} \, \mathbf{H} \, \mathbf{G}_{\mathcal{B}\text{T}} \, \mathbf{C} \, \mathbf{G}_{\mathcal{B}\text{R}}^{-1} \, |\mathbf{G}_{\mathcal{B}\text{R}}|^2 \, \mathbf{H}^H \left[\mathbf{H} \, |\mathbf{G}_{\mathcal{B}\text{R}}|^2 \, \mathbf{H}^H \right]^{-1} \mathbf{G}_{\mathcal{M}\text{T}}^{-1} \tag{7}$$

$$\mathbf{V}_{\text{WF}} = \mathbf{G}_{\mathcal{M}\text{R}} \, \mathbf{H} \, \mathbf{G}_{\mathcal{B}\text{T}} \, \mathbf{C} \, \mathbf{G}_{\mathcal{B}\text{R}}^{-1} \, |\mathbf{G}_{\mathcal{B}\text{R}}|^2 \, \mathbf{H}^H \left[\mathbf{H} \, |\mathbf{G}_{\mathcal{B}\text{R}}|^2 \, \mathbf{H}^H + \frac{\sigma_n^2}{P_\text{T}} \left(|\mathbf{G}_{\mathcal{M}\text{T}}|^2 \right)^{-1} \right]^{-1} \mathbf{G}_{\mathcal{M}\text{T}}^{-1} \tag{8}$$
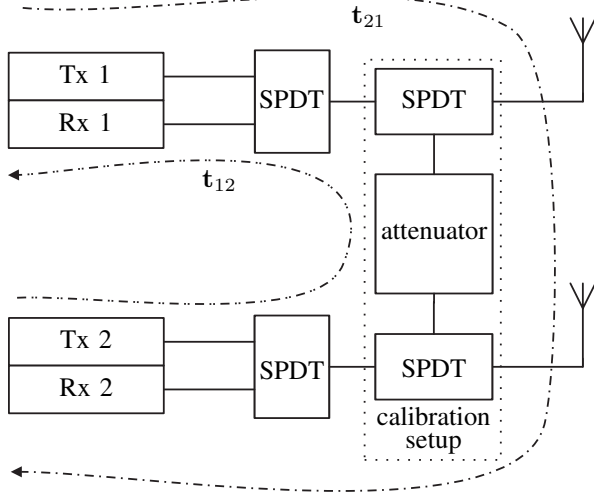

Fig. 1. Schematic of the two base station transceivers and the low-cost online calibration setup.

additional equalization at the receiver to compensate for the factor ζ_k. This results in a division of the noise component by ζ_k in (3).

III. SIMULATION RESULTS

The considered MU-MISO-OFDM system consists of 2 transmit and 2 receive antennas combined with $N_{\text{sc}} = 512$ subcarriers and a 4-QAM modulation scheme without channel coding is used. Additionally, the simulations are executed applying channel coding using a 3GPP punctured turbo code at code rate $R_c = 0.5$. To maintain the spectral efficiency of 2 bit/s/Hz of the uncoded 4-QAM, the modulation is adjusted to 16-QAM. The physical channel is modeled using a 6-tap Rayleigh-distributed channel impulse response (CIR) for each transmit-receive antenna pairing with equal power for each tap. Overall, the parameters were chosen to compare the simulation results with the measurement results obtained using the multiple antenna demonstrator. Since the focus is on a calibration of the base station, the effects of the transceivers of the MS are neglected in the simulations and therefore $\mathbf{G}_{\mathcal{M}\text{R}}$ and $\mathbf{G}_{\mathcal{M}\text{T}}$ reduce to identity matrices in (1) and (2), respectively. In contrast, the transceivers of the BS are modeled by allpass filters with gain factors $1 + \delta_k$ on each subcarrier k, with δ_k be-
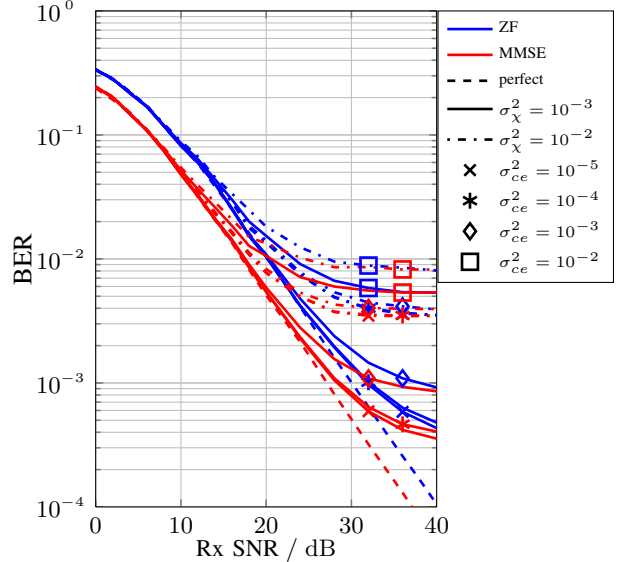

Fig. 2. Uncoded BER results with and without relative calibration at $\sigma_\delta^2 = -20$ dB.

ing a complex normal distributed random variable with variance σ_δ^2 [10]. In [9], the allpass filters are modeled using a uniformly distributed amplitude and uniformly distributed phase. From a physical point of view, the allpass filter models the baseband to baseband behavior of the transceivers. When using the proposed calibration procedure, two things have to be considered that may degrade the system performance, a calibration error and a channel estimation error (ce) of the UL channel matrix. The calibration error is modeled per subcarrier with respect to the calibration factors c_i by multiplying the c_i with $1+\chi_k$, where the χ_k is a complex normal distributed random variable with variance σ_χ^2. (11) describes the model used to include the effect of the channel estimation error [10]

$$\hat{\mathbf{H}}_{\text{UL},k} = \sqrt{1 - \sigma_{ce}^2} \cdot \mathbf{H}_{\text{UL},k} + \sqrt{\sigma_{ce}^2 \, (1 - \sigma_{ce}^2)} \cdot \mathbf{H}_{ce,k}, \tag{11}$$

where $\mathbf{H}_{ce}$ is a complex valued matrix with each entry being a complex normal distributed variable $\mathbf{H}_{ce} \in \mathcal{NC}(\mathbf{0}, \frac{1}{6} \mathbf{I})$.

Fig. 2 depicts the simulation results for uncoded data transmission. In conjunction with the channel estimation error, the impact of non-perfect calibration parameters on the BER has been evaluated. With a calibration error variance of $\sigma_\chi^2 = 10^{-3}$, the BER
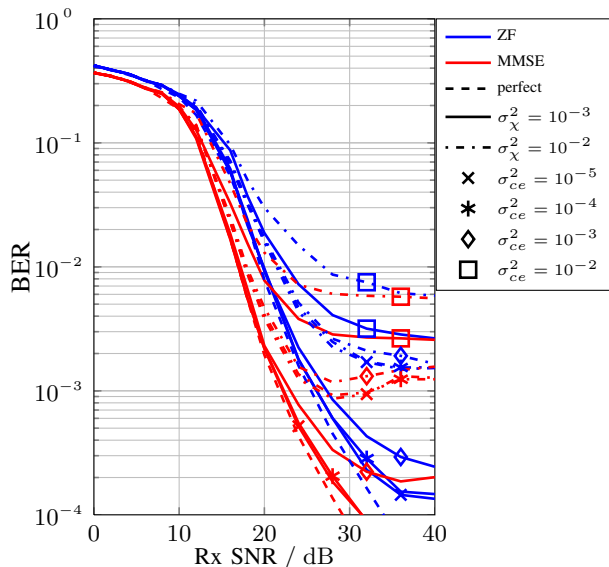
Fig. 3. Coded BER results with and without relative calibration at $\sigma_\delta^2 = -20$ dB.

Fig. 4. Measurement results of the magnitude of the reflection coefficients (S_{11}, S_{22}) and the transmission factors (S_{21}, S_{12}) and of the ratio between forward (S_{21}) and reverse path (S_{12}) of the calibration setup.

drops to a value of 10^{-3} as long as the channel estimation error remains smaller than $\sigma_{ce}^2 = 10^{-2}$ in the high SNR region without applied channel coding. Letting the calibration error jump to $\sigma_\chi^2 = 10^{-2}$, it is impossible to attain a BER of 10^{-3} for every assessed value of the channel estimation error, which is also the case for the combination $\sigma_\chi^2 = 10^{-3}$ and $\sigma_{ce}^2 = 10^{-2}$.

Considering the coded results depicted in Fig. 3, the curves are qualitatively comparable to the curves without applied channel coding (cf. 2). The main difference, as is expected, is an overall better performance with respect to the BER, which is smaller by approximately one order of magnitude at a calibration error of $\sigma_\chi^2 = 10^{-3}$ and a channel estimation error of $\sigma_{ce}^2 = 10^{-5}$ and $\sigma_{ce}^2 = 10^{-4}$. Important to note is that the MMSE pre-equalization outperforms the Zero Forcing pre-equalization more pronounced when applying channel coding. With an increasing channel estimation error the performance drops significantly to values similar to those obtained for raw data transmission. If the calibration error increases to $\sigma_\chi^2 = 10^{-2}$, the overall performance is unacceptable in terms of the BER. The latter does not get below the 10^{-3} mark. All in all, the calibration error has to be smaller than $\sigma_\chi^2 = 10^{-2}$ while keeping the channel estimation error at $\sigma_{ce}^2 = 10^{-3}$ or smaller to achieve acceptable results for this setup.

IV. Measurement Setup and Results

A measurement setup was proposed in [7] to evaluate the influence of non-reciprocal transceivers in a realistic environment. The former is taken and mo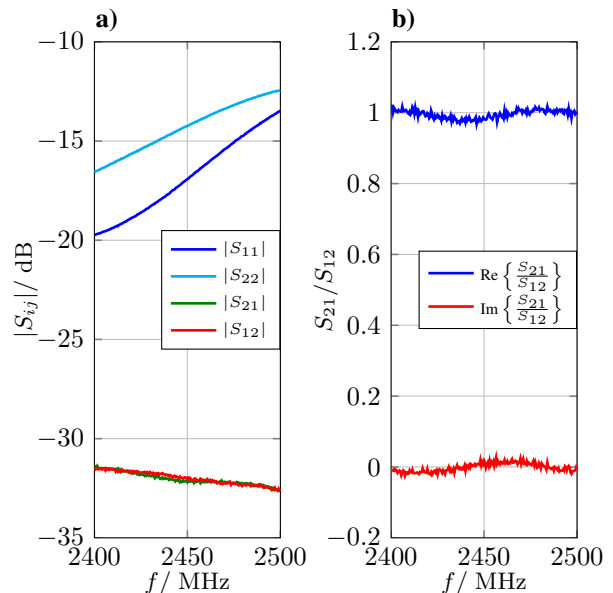dified according to Fig. 1, so that the hardware calibration setup can be exploited for a relative hardware-based calibration (HC) of the base station transceivers. The calibration setup consists of two SPDT switches and an attenuator as is depicted schematically in Fig. 1. The latter is needed to avoid overdriving the receiver chains of the base station transceivers. The simulations and the layout of the calibration setup was executed using the software suite Advanced Design System (ADS) by Agilent on an FR4 substrate with a thickness of 1.55 mm. The measurement results obtained using a network analyzer are depicted in Fig. 4 **a)**. Here, the indexes denote the respective transceivers of the base station including the duplexer. The matching at both ports is better than 12 dB and the attenuation is approximately 32 dB throughout the ISM band at 2.4 GHz. The attenuation factor was actually intended to be equal to 30 dB, but it is increased by approximately 2 dB because of the losses introduced by the FR4 substrate material. Fig. 4 **b)** depicts the real part and the imaginary part of the ratio between forward and reverse path of the calibration setup. A small ripple can be observed with respect to a mean value of $\mu_{cs} \approx 0.9956 - j\,0.0015$, which results in a variance of $\sigma_{cs}^2 \approx 2.76 \cdot 10^{-4}$. This ratio is an important figure of merit since it determines the achievable accuracy of the calibration procedure [4].

Fig. 5 shows the mean value and the variance of the measured allpass filter functions with respect to each subcarrier k of the transceivers of the multiple antenna demonstrator. The mean value of the variance σ_k^2 settles at $\sigma^2 = 2.2 \cdot 10^{-3} = -26.57$ dB.
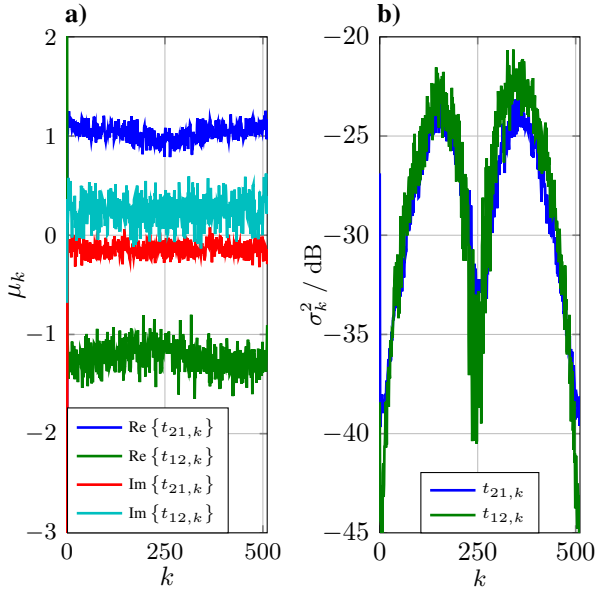
Fig. 5. Mean value μ_k (**a**) and variance σ_k^2 (**b**) of the base station's measured allpass filter functions of transmitter 1 to receiver 2 ($\mathbf{t}_{21}$) and transmitter 2 to receiver 1 ($\mathbf{t}_{12}$).

Fig. 6. Uncoded (**a**) and coded (**b**) BER results obtained exploiting the relative calibration at the base station in a line-of-sight (LOS) measurement scenario.

Interpreting the variance of the measured value as the calibration error, this value is slightly larger compared to the minimum value used in the simulations. Fig. 6 depicts the measurement results determined exploiting the multiple antenna demonstrator operating in a multiuser scenario. On the left hand side of Fig. 6, the uncoded results are depicted, which show an improvement of approximately 2.5 dB at a BER of 10^{-3} when applying the calibration parameters compared to the raw usage of the UL CSI. But there is still a gap of approximately 3.5 dB compared to the usage of the perfectly fed back DL CSI. A temperature dependency of the transceivers was observed in terms of the calibration parameters, which could not be compensated for due to the specific hardware setup. Fig. 6 **b)** shows the results when applying channel coding, which yield similar curves. At a BER of 10^{-3}, the hardware-based calibration outperforms the non-calibrated base station (UL CSI) by approximately 2.7 dB but it is inferior to the DL-CSI-based transmission by approximately 4 dB.

V. CONCLUSION

The simulation results as well as the measurement results show an improvement of the system performance in terms of the BER when exploiting the calibration parameters obtained with the help of our calibration setup. The benefit of this calibration scheme is its independence of the mobile subscribers. On the downside, additional hardware is ne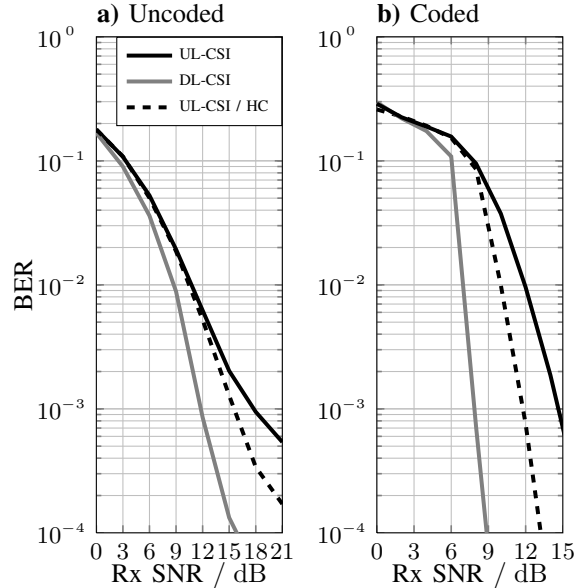eded although the calibration setup can be built using low-cost and simple technologies. To be able to improve the system performance closer to the performance achievable when exploiting DL CSI, signal processing based approaches need to be pursued.

REFERENCES

[1] J.G. Proakis and M. Salehi, *Digital Communications*, McGraw-Hill, fifth edition, 2008.

[2] A. E. Ekpenyong and Y.-F. Huang, "Feedback Constraints for Adaptive Transmission," *IEEE Signal Processing Magazine*, vol. 24, no. 3, pp. 69–78, May 2007.

[3] J. Liu, A. Bourdoux, J. Craninckx, P. Wambacq, B. Côme, S. Donnay, and A. Barel, "OFDM-MIMO WLAN AP Front-end Gain and Phase Mismatch Calibration," in *IEEE Radio and Wireless Conference (RAWCON)*, Atlanta, USA, Sept. 2004, pp. 151 – 154.

[4] J. Liu, G. Vandersteen, J. Craninckx, M. Libois, M. Wouters, and F. Petré, "A Novel and Low-cost Analog Front-end Mismatch Calibration Scheme for MIMO-OFDM WLANs," in *IEEE Radio and Wireless Symposium*, San Diego, USA, Apr. 2006, pp. 219–222.

[5] P. Zetterberg, "Experimental Investigation of TDD Reciprocity-Based Zero-Forcing Transmit Precoding," *EURASIP Journal on Advances in Signal Processing*, vol. 2011, 2011.

[6] J. Rinas, R. Seeger, L. Brötje, S. Vogeler, T. Haase, and K.-D. Kammeyer, "A Multiple-Antenna System for ISM-Band Transmission," *EURASIP Journal on Applied Signal Processing*, vol. 2004, no. 9, pp. 1407–1419, Aug. 2004.

[7] M. Stefer, M. Petermann, M. Schneider, D. Wübben, and K.-D. Kammeyer, "Influence of Non-Reciprocal Transceivers at 2.4 GHz in Adaptive MIMO-OFDM Systems," in *14th International OFDM-Workshop (InOWo) 2009*, Hamburg, Germany, 2009, pp. 143–147.

[8] C. Windpassinger, *Detection and Precoding for Multiple Input Multiple Output Channels*, Ph.D. thesis, University Erlangen-Nuremberg, Germany, 2004.

[9] W. Keusgen and B. Rembold, "Konzepte zur Realisierung von MIMO-Frontends," *Frequenz*, vol. 55, pp. 301–309, 2001.

[10] M. Petermann, M. Stefer, D. Wübben, M. Schneider, and K.-D. Kammeyer, "Low-Complexity Calibration of Mutually Coupled Non-Reciprocal Multi-Antenna OFDM Transceivers," in *7th International Symposium on Wireless Communication Systems (ISWCS 10)*, York, Great Britain, Sept. 2010, pp. 285 – 289.